Supplementary Information - Collective force generation by molecular motors is determined by strain-induced unbinding

Mehmet Can Uçar[1,2] and Reinhard Lipowsky[2]

[1] *Institute of Science and Technology Austria, Am Campus 1, 3400 Klosterneuburg, Austria*
[2] *Max Planck Institute of Colloids and Interfaces, Am Mühlenberg 1, 14476 Potsdam, Germany*

November 28, 2019

S1 Details of the fine-grained model

We briefly derive Eq. (2) of the main text, describe the single-motor properties, and provide a detailed description of the simulation algorithm.

S1.1 Elastic forces derived from force balance

We consider n active motors pulling a bead in the laser field of a stationary optical trap. The motors are attached to the bead with elastic linkers that act as harmonic springs with stiffness $\kappa_{\rm m}$, and the laser field is likewise represented as a harmonic spring with stiffness $\kappa_{\rm t}$. The elastic coupling between the laser field and the linkers of the motors can then be described in the framework of a tug-of-war between two teams of elastically interacting motors (1), where the optical trap represents a single immobile and active motor, *i.e.*, it is almost always attached to the track and almost never steps. The force balance condition between the motors and the laser field of the optical trap is given by (1)

$$\mathcal{F}_n \equiv \sum_{j=1}^{n} F_j \tag{S1}$$

where $\mathcal{F}_n$ is the overall instantaneous force acting on the optical trap, and

$$F_j \equiv \kappa_{\rm m} u_j \,, \tag{S2}$$

defines the elastic forces acting on individual motors. The elastic displacement

$$u_j \equiv L_j - L_\parallel \equiv x_j - x_{\rm be} - L_\parallel \tag{S3}$$

determines the extension of the $j-$th motor linker from the rest length $L_\parallel$, where x_j and $x_{\rm be}$ are the positions of the motor and the bead in a one-dimensional Cartesian coordinate system, respectively. The force acting on the optical trap can be similarly determined from the elastic displacement of a harmonic spring as

$$\mathcal{F}_n \equiv \kappa_{\rm t} u_{\rm t} \,, \tag{S4}$$

where

$$u_{\rm t} \equiv L_{\rm t} - L_\parallel \equiv x_{\rm be} - x_{\rm t} - L_\parallel \tag{S5}$$

is the spring displacement and the position of the trap wall is given by $x_{\rm t}$. Note that in our description all motors have positions $x_j > x_{\rm be}$ and the trap wall fulfils $x_{\rm t} < x_{\rm be}$. This assumption is reasonable

for describing processive motors that mainly perform successive forward steps starting from a relaxed configuration (1). Substituting Eqs. (S2-S5) into Eq. (S1) leads to the position of the bead

$$x_{\rm be} = \varphi \left[\kappa_{\rm t} x_{\rm t} + \kappa_{\rm m} \sum_{j=1}^{n} x_j + L_{\parallel} (\kappa_{\rm t} - n\kappa_{\rm m}) \right] , \tag{S6}$$

with the prefactor $\varphi \equiv (\kappa_{\rm t} + n\kappa_{\rm m})^{-1}$. Eq. (S6) implies that, when the position of the $j-$th motor x_j changes by several stepping events such that

$$x_j \to x_j' = x_j + s_j \, \ell \, , \tag{S7}$$

where s_j is an integer and ℓ is the step size of the motor, the bead position $x_{\rm be}$ will be shifted by a factor of $\kappa_{\rm m} \varphi \, s_j \, \ell$. We note that positive and negative values of s_j correspond to forward and backward steps of the motor, respectively. Taking into account all possible steps taken by any motor with label $j = 1, \ldots, n$, the overall shift in the bead position $x_{\rm be}$ after an arbitrary number of steps is then determined by

$$x_{\rm be} \to x_{\rm be}' = x_{\rm be} + \kappa_{\rm m} \varphi \sum_{j=1}^{n} s_j \, \ell \, . \tag{S8}$$

Substituting Eqs. (S7) and (S8) into Eq. (S3), the change in the elastic displacement of the $j-$th motor is given by

$$\begin{aligned} u_j \to u_j' &= x_j' - x_{\rm be}' - L_{\parallel} \\ &= u_j + s_j \, \ell \, (1 - \kappa_{\rm m} \varphi) - \kappa_{\rm m} \varphi \sum_{\substack{k=1 \\ k \neq j}}^{n} s_k \, \ell \, . \end{aligned} \tag{S9}$$

We define a *relaxed reference state* with $u_j = 0$ for all active motors j, and assume that the minimal strain state in the system will be described by this relaxed state (1), *i.e.*, all active motors can attain positions on the track such that their linkers are relaxed. The step numbers s_j are then identified as distances from this relaxed reference state measured in units of the step size ℓ. Starting from this relaxed state, after any arbitrary number of steps taken in the system, the force acting on the $j-$th motor given by Eq. (S2) thus becomes

$$F_j = 0 \to F_j' = \kappa_{\rm m} \, \ell \left[(1 - \kappa_{\rm m} \varphi) \, s_j - \kappa_{\rm m} \varphi \sum_{\substack{k=1 \\ k \neq j}}^{n} s_k \right] . \tag{S10}$$

Eq. (S10) thus describes elastic forces acting on each motor in all accessible configurations determined by the set of step numbers $\{s_1, \ldots, s_n\}$, as given by Eq. (2) of the main text. We note that, in the tug-of-war framework (1), the single motor that represents the optical trap can also take forward and backward steps. Therefore, there is in general an extra term in Eq. (S10) that corresponds to the "steps" of the trap. However, we adjust the corresponding trap parameters such that these events are extremely rare and we can assume $s_{\rm t} \simeq 0$ at any time step.

S1.2 Single motor description

The description of a single motor is based on a previous work developed in Ref. (2). The motion of the motor on the track is described as a random walk with forward and backward stepping rates α and β, respectively. The stepping rates are force-dependent and can be used to define the force-dependent velocity *via* the relation $\alpha(F) - \beta(F) = v(F)/\ell$, where ℓ is the step size of the motor. In the absence of

an external force acting on the motor, the motor moves with its zero-force velocity $v(F=0)=v_0$. The velocity decreases monotonically with increasing external force until the stall force F_s is reached where the motor velocity becomes zero, *i.e.*, the motor steps forward and backward with equal probability at F_s due to $\alpha(F_s)-\beta(F_s)=v(F_s)/\ell=0$. If the force exceeds the stall force, *i.e.*, for $F>F_s$, the motor moves backwards with the average velocity $-v_{\min}$ for large F. For assisting forces, *i.e.*, for $F<0$, the motor reaches its maximal forward velocity $v_{\max}$ for large negative values of F. We use the following parametrization for the force-velocity relation of a single motor (2, 3)

$$v(F)=\frac{v_{\max}\frac{v_{\min}-v_0}{v_0-v_{\max}}+v_{\min}\left(\frac{v_{\max}}{v_{\min}}\frac{v_0-v_{\min}}{v_0-v_{\max}}\right)^{F/F_s}}{\frac{v_{\min}-v_0}{v_0-v_{\max}}+\left(\frac{v_{\max}}{v_{\min}}\frac{v_0-v_{\min}}{v_0-v_{\max}}\right)^{F/F_s}}\,. \tag{S11}$$

The force-dependent stepping rates of the motor are defined by

$$\alpha(F)\equiv\frac{v(F)}{\ell}\,\frac{q(F)}{q(F)-1}\,,\quad\text{and}\quad\beta(F)\equiv\frac{v(F)}{\ell}\,\frac{1}{q(F)-1}\,, \tag{S12}$$

where $q(F)$ is the forward-to-backward stepping ratio fitted by (4, 2)

$$q(F)=q_0^{1-F/F_s}\,, \tag{S13}$$

with the zero-force stepping ratio q_0.

In the absence of an external force, a processive motor unbinds from the filament due to thermal fluctuations with a zero-force unbinding rate ϵ_0. This rate can be obtained experimentally using the relation $\epsilon_0=\langle v\rangle/\langle x\rangle$, where $\langle v\rangle=v_0$ is the average zero-force velocity and $\langle x\rangle$ is the average run length of the motor. If an external force acts on the motor, the unbinding can be described as an escape process of a particle in a potential well (5) with the force-dependent unbinding rate given by

$$\epsilon(F)=\epsilon_0\exp(|F|/F_d)\,, \tag{S14}$$

where F_d is the detachment force. The latter force scale is determined by the energy barrier between the bound and the unbound states of the motor. In most theoretical studies this force value is assumed to be on the order of $F_d\simeq 3\,\mathrm{pN}$ (6), although recent experimental (7) and theoretical studies (8) for kinesin-1 estimated a value of about $6-7\,\mathrm{pN}$. However, we note that in Ref. (7), the force-dependent unbinding rate was fitted for force ranges that are much larger than the stall force of kinesin-1. Therefore, we used their estimate from a fit to the force-dependent run length within the stall force regime, which implies a value of $F_d\simeq 2.1\,\mathrm{pN}$, see Table S1.

An unbound (inactive) motor can rebind to the filament when it comes in close proximity to it such that the distance between the motor domain and the filament is comparable to the rest length of the motor linker. This rebinding event can be assumed to be independent of the forces acting on the bead because the unbound motor linker relaxes much faster than the movement of the bead. Therefore, we assign a constant rate $\pi(F)=\pi_0$ for the rebinding of the unbound motor to the filament. In general, this rate depends on the buffer conditions or on the geometric arrangement of the motor assembly, and can influence the collective behavior of motor teams. In section S5 below, we investigate the changes in the collective force generation by adjusting these single motor parameters one at a time.

Note that a full set of parameters for each studied motor type has not been found in the existing experimental studies, see Table S1. We therefore employ the following strategy for the missing parameters: In general, the missing parameters take the values corresponding to those of kinesin-1 because the latter is the most extensively studied motor type. For the step ratio q_0 of weak dynein and the unbinding rate ϵ_0 of strong dynein, however, we assigned the available values from the other dynein motor because these two motors are closely related. Another exception is the stiffness κ of the two

Parameter	kinesin-1	dynein (S)	dynein (W)	kinesin-5	myosin-5a	myosin-6	optical trap
Unbinding rate ϵ_0 [s^{-1}]	0.66 (7)	1*	1 (9)	0.66*	0.34 (10)	0.25 (10)	0.001
Binding rate π_0 [s^{-1}]	5 (11), 2‡	5*	5*	5*	5*	5*	50
Stall force F_s [pN]	7 (4)	7 (12, 13)	1.1 (14, 15)	1.5 (16, 17)	2.5 (18, 19, 20)	2.2 (21)	20
Detachment force F_d [pN]	2.1 (7)	2.9 (22)	2.9 (22)	2.1*	2.1*	2.1*	50
Stiffness κ [pN/nm]	0.2 (23)	0.05 (24)	0.05 (24)	0.2*	0.05*	0.05*	$\kappa_{\rm m}$
Step size ℓ [nm]	8 (4, 23)	8 (25)	8 (12)	8 (26)	36 (18, 10)	36*	$\ell_{\rm m}$
Step ratio q_0	800 (4)	4 (25)	4*	800*	800*	800*	10
Velocity v_0 [nm/s]	740 (7)	85 (25)	800 (12)	30 (16)	378 (10)	146 (10)	5
Min. velocity $v_{\rm min}$ [nm/s]	89†	10†	96†	3.6†	45†	18†	0.1
Max. velocity $v_{\rm max}$ [nm/s]	829†	95†	896†	33.6†	423†	164†	5.1

Table S1: Values of the parameters used for the molecular motors investigated in the main text: The values for "strong" and "weak" dynein (columns dynein (S) and dynein (W)) correspond to yeast and mammalian cells, respectively. For kinesin-1 motors that we used to compare our theoretical calculations with the experimental data in Ref. (27), see Fig. 4 of the main text and section S3 below, we only modified the binding rate π_0. The corresponding value is indicated by the double-dagger superscript. For the stall force of myosin-5a, a range of values between 2-3 pN were reported in Refs. (18, 19, 20). We therefore used an estimated value of $F_s = 2.5\,$pN. An asterisk superscript indicates a parameter for which we did not find experimental data in the literature; the corresponding parameter value was set equal to the experimentally determined value of another type of motor. Velocity values depicted by the dagger superscript are estimated by $v_{\rm min} \simeq 0.12\,v_0$ and $v_{\rm max} \simeq 1.12\,v_0$. The parameters for the optical trap were chosen to resemble a motor which is (almost) immobile and does not detach from the filament. The stiffness and step size values for the optical trap indicated by $\kappa_{\rm m}$ and $\ell_{\rm m}$, respectively, are identical to the motor type that pulls on it.

myosin motors. For this parameter, choosing kinesin-1's value ($\kappa = 0.2\,$pN/nm) combined with the rather large step size of the myosin motors ($\ell = 36\,$nm) leads to a force generation of $F = \frac{\kappa}{2}\ell = 3.6\,$pN after each step for the case of a single bound motor ($n = 1$). This force scale exceeds the stall force of both myosin motors and thus the simulation cannot provide reliable statistics to obtain force distributions. Therefore, we chose the value corresponding to the stiffness of dynein motors ($\kappa = 0.05\,$pN) for the two myosin motors.

S1.3 Details of the simulation

For each simulation run, we first fix the number of available motors N in the system, and then start the simulation in an activity state (n) with $n = N$, *i.e.*, where all available motors are attached to the filament. We start from the relaxed state $\mathbf{u}_0 = (u_1 = 0, \ldots, u_n = 0)$ where all motors have relaxed linkers with step numbers given by $\{s_1 = 0, \ldots s_n = 0\}$. The simulation based on Gillespie algorithm then follows the following steps:

(i) Elastic forces F_j acting on the active motors given by Eq. (S10) determine all force-dependent transition rates of each active motor j *via* Eqs.(S11-S14). We draw a random number r_d in the unit interval $[0,1]$ and calculate an exponentially distributed dwell time for configuration $\mathbf{u} = (u_1, u_2, \ldots, u_n)$ (with step numbers $\{s_1 \ldots, s_n\}$) by $\tau_{\mathbf{u}} \equiv (-1/\sum_{\mathbf{u}'} \omega_{\mathbf{u}\to\mathbf{u}'}) \ln(r_d)$, where $\omega_{\mathbf{u}\to\mathbf{u}'}$ represents the transition rate into a new configuration $\mathbf{u}'$ that can be realized by the stepping, unbinding and rebinding events of any motor. The dwell time $\tau_{\mathbf{u}}$ is recorded as the time spent at configuration $\mathbf{u}$.

(ii) Probabilities $\Pi_{\mathbf{u}\to\mathbf{u}'}$ for each transition $\mathbf{u} \to \mathbf{u}'$ are obtained by dividing the corresponding transition rate by the sum of rates for all possible transitions, *i.e.*, $\Pi_{\mathbf{u}\to\mathbf{u}'} \equiv \omega_{\mathbf{u}\to\mathbf{u}'}/\sum_{\mathbf{u}'} \omega_{\mathbf{u}\to\mathbf{u}'}$. We then order the transition probabilities cumulatively as $[0, \Pi_{\mathbf{u}\to\mathbf{u}'}, \Pi_{\mathbf{u}\to\mathbf{u}'} + \Pi_{\mathbf{u}\to\mathbf{u}''}, \ldots, \sum_{\mathbf{u}'} \Pi_{\mathbf{u}\to\mathbf{u}'}]$.

(iii) We draw another random number r_t that determines the transition into the next configuration. If the number lies within the interval $[\Pi_{\mathbf{u}\to\mathbf{u}'}, \Pi_{\mathbf{u}\to\mathbf{u}'} + \Pi_{\mathbf{u}\to\mathbf{u}''}]$ the next transition is determined as a transition into the configuration $\mathbf{u}''$ with new step numbers $\{s_1'', \ldots, s_n''\}$. Note that the unbinding and rebinding events can change the number of active motors n at each time step.

(iv) Return to step (i) to update all elastic forces F_j *via* the new set of step numbers and the corresponding transition rates.

An important issue concerns the position on the track where a detached motor rebinds to: In general, one should assume that the motor linker is in a relaxed configuration after rebinding events, such that the overall instantaneous force remains unchanged, *i.e.*, $\mathcal{F}_{n-1} = \mathcal{F}_n$ where n denotes the number of active motors after the rebinding event. This force balance argument implies that, see Eq. (S1),

$$\sum_{j=1}^{n-1} F_j = \sum_{j=1}^{n} F_j \,, \tag{S15}$$

where F_j is the elastic force experienced by the j-th active motor. Substituting Eq. (S10) for the left- and right-hand sides of Eq. (S15), we obtain

$$\frac{\kappa_\mathrm{t}}{\kappa_\mathrm{t} + (n-1)\kappa_\mathrm{m}} \sum_{j=1}^{n-1} s_j = \frac{\kappa_\mathrm{t}}{\kappa_\mathrm{t} + n\kappa_\mathrm{m}} \sum_{j=1}^{n} s_j \,, \tag{S16}$$

which imposes the following condition on the step number of the $k = n$-th motor that rebinds to the track

$$s_k = \frac{\kappa_\mathrm{m}}{\kappa_\mathrm{t} + (n-1)\kappa_\mathrm{m}} \sum_{j=1}^{n-1} s_j \,. \tag{S17}$$

For $\kappa_\mathrm{t} = \kappa_\mathrm{m}$, this expression simplifies to

$$s_k = \frac{1}{n} \sum_{j=1}^{n-1} s_j \,, \tag{S18}$$

which corresponds to the case in our simulations. Note that, however, Eq. (S18) does not always represent an integer for the step number s_k. In such cases, we round the value for s_k to the nearest integer, which induces a change in the overall instantaneous force by at most $\Delta\mathcal{F}_n = \pm\frac{1}{2}\kappa_\mathrm{m}\ell$.

We repeat each simulation run until the overall dwell time of the process reaches $T \equiv \sum_{\mathbf{u}} \tau_{\mathbf{u}} = (N+2) \times 100\,\mathrm{s}$, *i.e.*, the simulation runs increase linearly with the number N of available motors in the system to avoid small sample sizes. For long simulation runs, we then record and sum over the random dwell times $\tau_{\mathbf{u}}$ for each configuration $\{s_1, \ldots, s_n\}$, and estimate its steady state probability $p^{\mathrm{st}}\{s_1, \ldots, s_n\}$ by the summed dwell times normalized by the total time T of the simulation. We regard the probabilities $p^{\mathrm{st}}\{s_1, \ldots, s_n\}$ as frequencies for the overall force $\mathcal{F}_n$ at that configuration, and thus obtain force distributions for a fixed number N of available motors in every simulation.

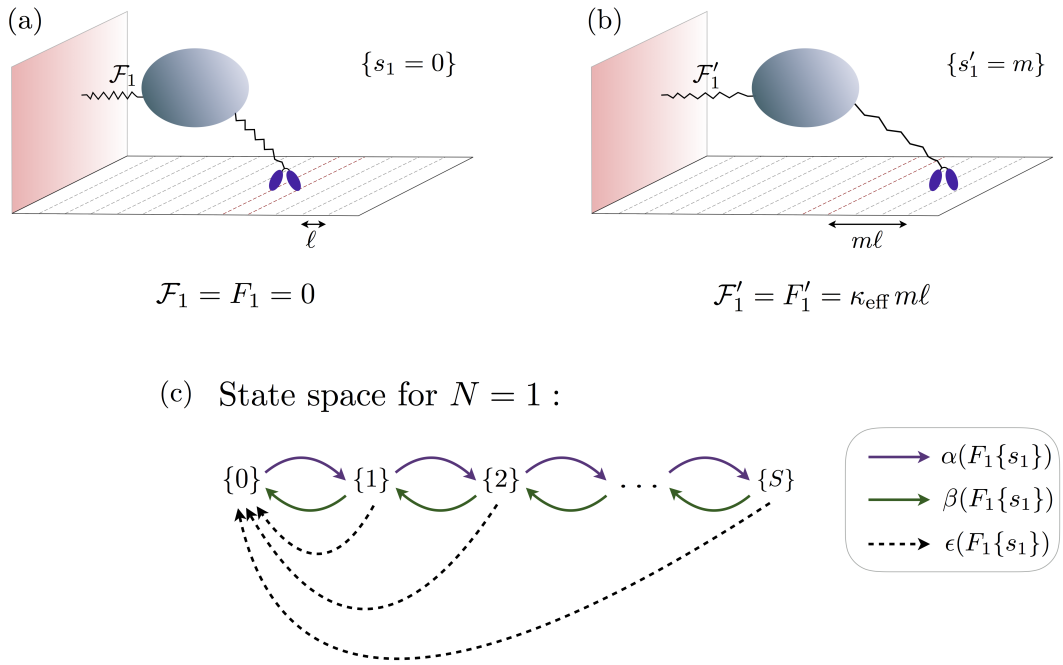

Figure S1: Elastic states of a single motor in a stationary optical trap. Cartoons depict (a) the relaxed state $\{s_1 = 0\}$ where the length of the motor linker corresponds to its rest length, and thus the forces acting on the motor and on the optical trap vanish; and (b) the stretched state $\{s_1' = m\}$ where the motor is m steps away from the relaxed state $\{s_1 = 0\}$. The elastic forces acting on the trap and on the motor, determined by Eqs. (S1) and (S10), respectively, are given by $\kappa_{\rm eff}\, m\ell$ with the effective spring constant $\kappa_{\rm eff} \equiv \kappa_{\rm t}\kappa_{\rm m}/(\kappa_{\rm t} + \kappa_{\rm m})$. (c) Complete state space of the single motor system. Elastic states $\{s_1\}$ with the step number $s_1 = 0, \ldots, S$ correspond to different extensions of the motor linker. Transitions that stretch the motor linker, *i.e.*, $\{s_1'\} \to \{s_1' + 1\}$ are governed by the forward stepping rate $\alpha(F_1\{s_1\})$, and transitions that relax the motor linker, *i.e.*, $\{s_1'\} \to \{s_1' - 1\}$ are determined by $\beta(F_1\{s_1\})$. Unbinding of the motor from the track is governed by the unbinding rate $\epsilon(F_1\{s_1\})$ (broken lines). We assume that, once detached, the motor instantaneously rebinds to the relaxed state $\{s_1 = 0\}$.

S2 Details of the coarse-grained model

Here we describe the coarse-grained (CG) model that determines the estimated average forces $\langle \mathcal{F}_N^* \rangle$ plotted in Figs. 3(a1-a3) and Fig. 6 of the main text. Similar to the fine-grained (FG) model, the CG model includes activity states (n) with different numbers $n = 0, \ldots, N$ of active motors, and elastic substates $\mathbf{u} = (u_1, \ldots, u_n)$ that describe the elastic extensions of the motor linkers. In the FG model, each active motor can take an arbitrary number s_j of steps such that the elastic linkers of the active motors can have different lengths at any time. Because of n independent step numbers, the complete state space in the FG model consists of 2^N activity states (n) that have n-dimensional elastic substates $\{s_1, \ldots, s_n\}$. The different elastic substates are connected by the forward and backward stepping events, whereas any transition between elastic substates of two different activity states are governed by unbinding and rebinding events.

The CG model simplifies this FG state space by reducing the n-dimensional elastic subspace of each activity state (n) into a 1-dimensional state space. This reduction is based on the approximation that during force generation all active motors share the overall force acting on the trap equally at any instance. The transitions between different activity states (n) are then governed by *effective* rebinding and unbinding rates that depend on the average forces generated in each activity state. In particular, the CG algorithm is based on the following steps:

(i) Calculate the average force of a single motor: To reduce the fine-grained state space of N available

motors, we first consider the elastic force generation of a single available motor ($N = 1$) against the optical trap. The state space of such a system was developed previously to describe two elastically coupled identical and antagonistic motors in Refs. (2) and (3), respectively. The single motor can step along the filament and thus generate elastic forces by extending its motor linker. These elastic states are represented as $\{s_1\}$ with the step number $s_1 = 0, 1, \ldots, S$, where S is a large integer. In principle, the step number s_1 can also take negative values, corresponding to motor positions that are accessible *via* backward stepping events starting from the relaxed reference state $\{s_1 = 0\}$. However, these configurations are extremely rare and for simplicity we omit these states in the description. Forward transitions $\{s_1\} \to \{s_1 + 1\}$ that stretch the motor linker are governed by the forward stepping rate $\alpha(F_1\{s_1\})$, and backward transitions $\{s_1\} \to \{s_1 - 1\}$ that relax the motor linker by the backward stepping rate $\beta(F_1\{s_1\})$. These transition rates are determined by Eqs. (S12), whereas the force $F_1\{s_1\} \equiv F_1$ that depends on the elastic state $\{s_1\}$ can be calculated from Eq. (S10) for $n = 1$. We furthermore make the assumption that once detached, the motor instantaneously rebinds to the relaxed state $\{s_1' = 0\}$ such that transitions into the relaxed state are governed by the rate $\epsilon(F_1\{s_1\})$, see Eq. (S14). The complete state space of the single motor system is depicted in Fig. S1. To obtain the steady state probabilities $p^{\mathrm{st}}\{s_1\}$ for the elastic substates, we numerically solve the master equation corresponding to this state space and determine the average elastic forces $\langle F_1 \rangle$ as described in Ref. (3). By Eq. (S1) we then have $\langle \mathcal{F}_1^* \rangle = \langle F_1 \rangle$, where $\langle \mathcal{F}_1^* \rangle$ is the average force acting on the optical trap. We use the asterisk superscript for the forces obtained using the CG algorithm.

(ii) Define coarse-grained elastic substates for each activity state: We now use the average single motor force $\langle \mathcal{F}_1^* \rangle$ obtained in (i) to describe the elastic substates of the activity states (n) with $n > 1$. First we redefine the single motor stall force as $F_s' \equiv \langle \mathcal{F}_1^* \rangle$, which indicates that each active motor will have equal probabilities of forward and backward stepping at the single motor *average* force, *i.e.*, $\alpha(\langle \mathcal{F}_1^* \rangle) = \beta(\langle \mathcal{F}_1^* \rangle)$. We then impose the condition that active motors share their overall load equally at any elastic substate. Each motor then experiences the force $\mathcal{F}_n/n$, where $\mathcal{F}_n$ is the instantaneous force acting on the optical trap. Using Eqs. (S1) and (S10), we obtain the elastic forces acting on individual motors as

$$F\{\sigma_n\} \equiv \mathcal{F}_n/n = \frac{\kappa_{\mathrm{t}}\kappa_{\mathrm{m}}}{\kappa_{\mathrm{t}} + n\kappa_{\mathrm{m}}}\, \ell\, \sigma_n\,, \tag{S19}$$

where $\sigma_n \equiv \frac{1}{n}\sum_{j=1}^{n} s_j$ is the effective step number that corresponds to different extensions of motor linkers. The elastic substates of any activity state (n) are then described by a single variable $\sigma_n = 0, \frac{1}{n}, \frac{2}{n}, \ldots, S$. In this elastic subspace a forward transition $\{\sigma_n\} \to \{\sigma_n + \frac{1}{n}\}$ is governed by the effective forward stepping rate $n\alpha(F\{\sigma_n\})$, whereas a backward transition $\{\sigma_n\} \to \{\sigma_n - \frac{1}{n}\}$ is governed by $n\beta(F\{\sigma_n\})$. We do not include unbinding or rebinding of the motors such that the elastic subspace of each activity state (n) forms a one-dimensional state space. The latter condition enforces detailed balance on the elastic subspace, thus the steady state probabilities $p^{\mathrm{st}}\{\sigma_n\}$ for the different substates $\{\sigma_n\}$ can be obtained recursively from the ratio of products of forward and backward stepping rates (28). From these probabilities we obtain the average CG-forces $\langle \mathcal{F}_n^* \rangle$ for each distinct activity state (n) with $n > 1$. Because of the redefined stall force $F_s' = \langle \mathcal{F}_1^* \rangle$ and detailed balance, the CG-forces of each activity state are normally distributed around the average forces $\langle \mathcal{F}_n^* \rangle = n\langle \mathcal{F}_1^* \rangle$.

(iii) Determine the probabilities of distinct activity states: We now reconnect the distinct activity states of the CG model by defining the effective unbinding rate $\epsilon(n) \equiv n\epsilon(\langle \mathcal{F}_n^* \rangle/n) = n\epsilon(\langle \mathcal{F}_1^* \rangle)$ and rebinding rate $\pi(n) \equiv (N - n)\pi_0$. The former rate describes transitions $(n) \to (n - 1)$ and the latter corresponds to transitions $(n) \to (n + 1)$. Therefore, the network of activity states is also one-dimensional and obeys detailed balance such that the steady state probabilities $P^{\mathrm{st}}(n)$

for the different activity states can be obtained as a ratio of products of the effective rates $\epsilon(n)$ and $\pi(n)$.

(iv) Reweight the probabilities of all elastic substates: The steady state probabilities $P^{\rm st}(n)$ for the activity states are then used to reweight the probabilities $p^{\rm st}\{\sigma_n\}$ for the elastic substates of each activity state. We finally use the reweighted probabilities

$$\hat{p}^{\rm st}\{\sigma_n\} \equiv P^{\rm st}(n) p^{\rm st}\{\sigma_n\} \tag{S20}$$

to obtain the overall coarse-grained average force $\langle \mathcal{F}_N^* \rangle$ for a fixed number N of available motors.

S2.1 Exemplary state space for $N = 2$

To illustrate the difference between the FG and the CG model, we consider a system with $N = 2$ available motors, as depicted in Fig. S2(a) and (b). This system consists of 4 distinct activity states (0), $(1)_1$, $(1)_2$, and (2) with $n = 0, 1$ or 2 motors attached to the track. Note that we distinguish each motor by the subscript $j = 1, 2$.

Fine-grained forces. The elastic substates $\{s_1\}$ of the activity state $(1)_1$ where the motor 1 is bound to the track are described by the step number s_1 which determine the distance of motor 1 from the relaxed state $\{0\}$ in units of the step size ℓ. As the motor performs successive steps, the elastic force F_1 acting it changes by

$$F_1 = \kappa_{\rm m}\ell(1 - \kappa_{\rm m}\varphi)s_1 = \frac{\kappa_{\rm t}\kappa_{\rm m}}{\kappa_{\rm t} + \kappa_{\rm m}}\,\ell s_1\,, \tag{S21}$$

in activity state $(1)_1$, as follows from Eq. (S10). The elastic forces acting on motor 2 in the activity state $(1)_2$ are obtained analogously. In the activity state $(n = 2)$, on the other hand, the elastic substates form a 2-dimensional state space $\{s_1, s_2\}$ with the two independent step numbers s_1 and s_2. The elastic forces acting on motor 1 and 2 are then expressed by

$$F_1 = \varphi\,\kappa_{\rm m}\ell\,((\kappa_{\rm t} + \kappa_{\rm m})s_1 - \kappa_{\rm m}s_2)\,, \quad \text{and} \tag{S22}$$

$$F_2 = \varphi\,\kappa_{\rm m}\ell\,((\kappa_{\rm t} + \kappa_{\rm m})s_2 - \kappa_{\rm m}s_1)\,, \tag{S23}$$

respectively, such that at any elastic substate $\{s_1, s_2\}$ the instantaneous force acting on the optical trap is given by

$$\mathcal{F}_2 = F_1 + F_2 = \varphi\,\kappa_{\rm t}\kappa_{\rm m}\ell(s_1 + s_2)\,, \tag{S24}$$

with $\varphi = (\kappa_{\rm t} + 2\kappa_{\rm m})^{-1}$, as follows from Eqs. (S1) and (S10). Note that, in general, the force-dependent transition rates $\alpha(F_j)$, $\beta(F_j)$ and $\epsilon(F_j)$ can be different for each motor j in the activity state (2) if the forces are not equal, *i.e.*, $F_1 \neq F_2$, see Fig. S2(a). We also emphasize that, in the fine-grained description, the activity state (2) consists of $(S+1)^2$ elastic substates $\{s_1, s_2\}$ where $s_j = 0, \ldots, S$ and S is a large integer. In any arbitrary elastic substate $\{s_1', s_2'\}$ one of the two motors can unbind from the filament, leading to a transition into one of the elastic substates of the activity states $(1)_1$ or $(1)_2$. Therefore, the fine-grained state space has a nested structure with many transitions between elastic substates of the different activity states.

Coarse-grained state space. In contrast with the fine-grained model, in the coarse-grained model we first describe the elastic substates of the distinct activity states individually, and subsequently reconnect the distinct activity states by effective transition rates, see steps (i-iv) above. For the case of $N = 2$ available motors, the coarse-grained model includes the two activity states $(n = 2)$ and $(n = 1)$

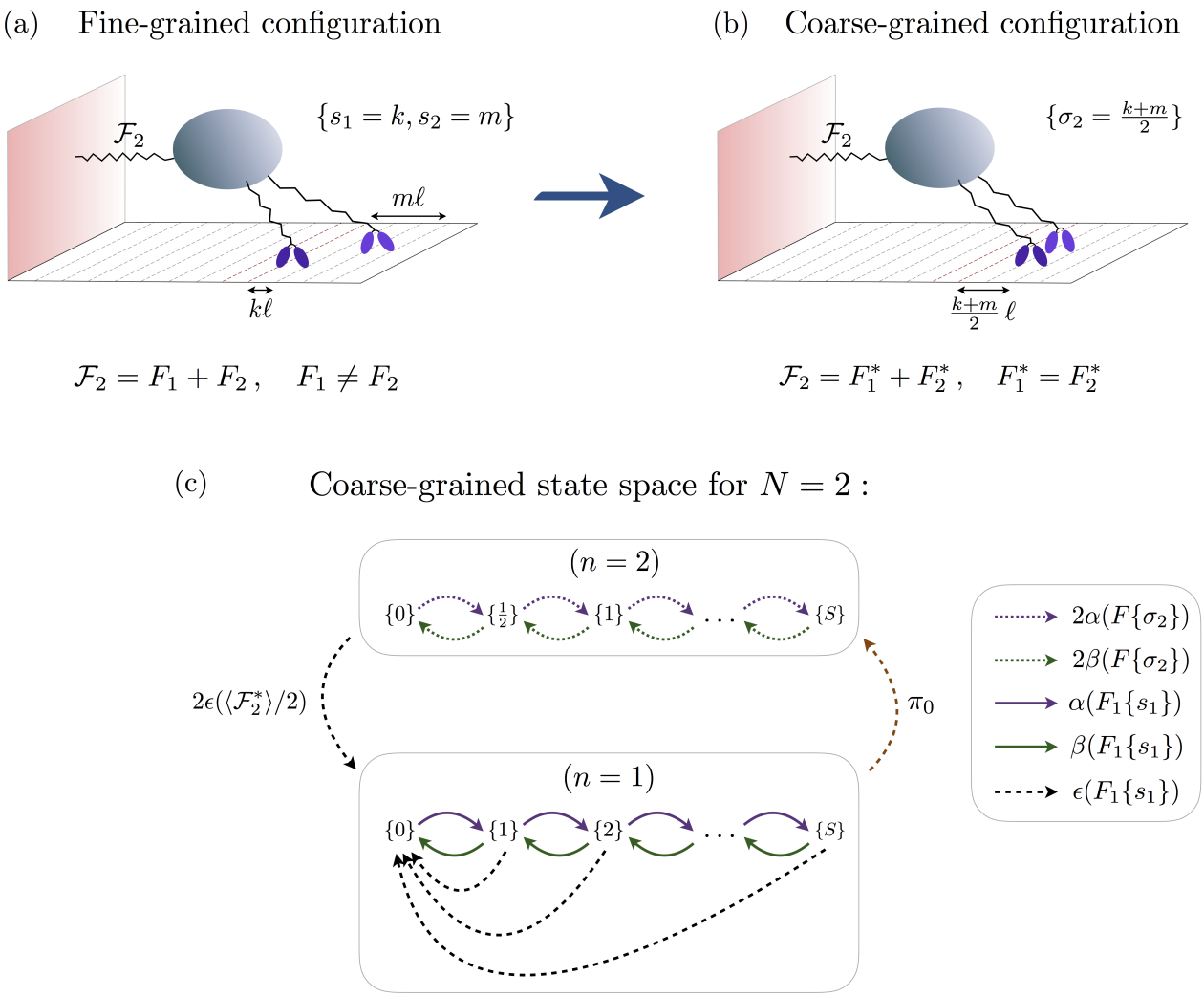

Figure S2: Depiction of the coarse-graining algorithm for a system of $N = 2$ available motors. (a) The fine-grained description of a configuration with two active motors with unequal step numbers, *i.e.*, $s_1 \neq s_2$, as represented here with $s_1 = k < s_2 = m$. The motors have different distances $k\ell$ and $m\ell$ from the relaxed state $\{0, 0\}$, thus the elastic forces F_1 and F_2 acting on the individual motors, see Eq. (S10), take different values. The overall force acting on the optical trap $\mathcal{F}_2$ is given by the sum of the two elastic forces. (b) The coarse-grained model describes the configuration depicted in (a) by averaging over the step numbers $s_1 = k$ and $s_2 = m$ into a single effective step number $\sigma_2 = \frac{k+m}{2}$. The motors therefore have the same distance from the relaxed state and experience the same elastic force $F_1^* = F_2^*$, where the asterisk superscript indicates the coarse-grained forces. (c) State space of the system with $N = 2$ available motors in the coarse-grained model. Transitions between substates $\{\sigma_2\}$ of the activity state $(n = 2)$ are governed by the forward and backward stepping rates, see inset. Transitions betweeen the activity states $(n = 2)$ and $(n = 1)$ are determined by the rebinding rate π_0 and the effective unbinding rate $2\epsilon(\langle\mathcal{F}_2^*\rangle/2)$, where $\langle\mathcal{F}_2^*\rangle = 2\langle\mathcal{F}_1\rangle$ is the average force generated in the activity state $(n = 2)$. The average single motor force $\langle\mathcal{F}_1\rangle$ is determined by the elastic state space corresponding to the activity state $(n = 1)$, see Fig. S1, which has the same value in the fine-grained and coarse-grained models.

that describe the elastic forces generated by a single or two active motors, respectively. The activity state (2) consists of elastic substates $\{\sigma_2\}$, where $\sigma_2 = \frac{s_1+s_2}{2}$ is the effective step number that takes the values $\sigma_2 = 0, \frac{1}{2}, 1, \ldots, S$. Eq. (S19) determines the elastic forces acting on each motor j in state $\{\sigma_2\}$ as

$$F_j^* \equiv F\{\sigma_2\} = \frac{\kappa_\mathrm{t}\,\kappa_\mathrm{m}}{\kappa_\mathrm{t} + 2\kappa_\mathrm{m}}\,\ell\sigma_2\,, \tag{S25}$$

where we used the asterisk superscript to indicate the coarse-grained forces acting on single motors. The instantaneous force acting on the optical trap is then given by $\mathcal{F}_2 = F_1^* + F_2^* = 2F\{\sigma_2\}$, *i.e.*, each bound motor experiences the same elastic force in each substate $\{\sigma_2\}$. Transitions corresponding

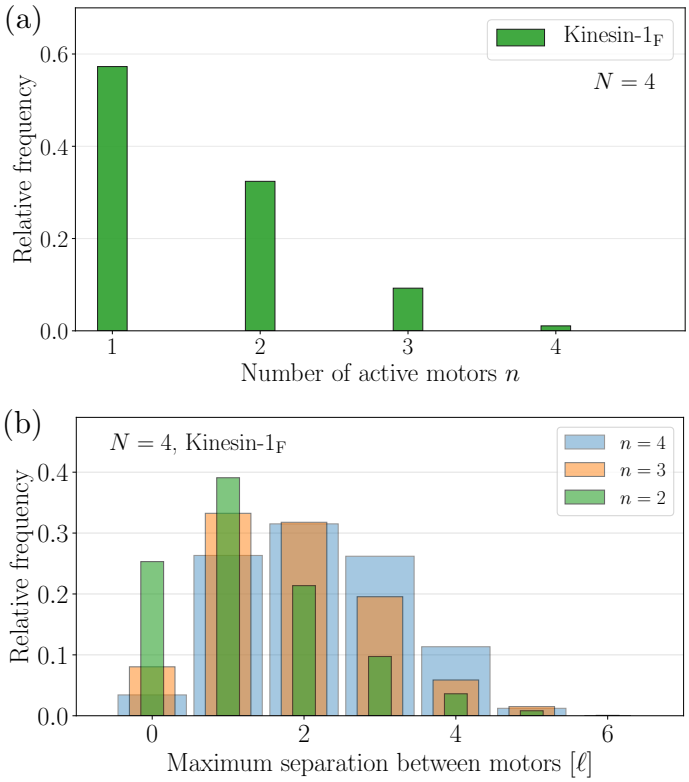

Figure S3: Details of the simulation data for $N = 4$ available motors in a stationary optical trap corresponding to Fig. 4 of the main text. Parameter values correspond to kinesin-1, where the only modified parameter is the binding rate π_0, see Table S1. (a) Relative frequencies for the different activity states with n active motors pulling the bead. The probabilities strongly decrease for large n, which indicate that the collective forces of $N = 4$ available kinesin-1 motors are mainly generated by one or two active motors. (b) Relative frequencies for the maximum separation between the leading and the trailing motor for $n = 2, 3, 4$ active motors attached to the track. The distributions indicate that active motors are typically separated by at most 2 steps.

to the stretching of the linkers of both active motors are then governed by the forward stepping rate $2\alpha(F\{\sigma_2\})$, and transitions for the relaxation of the motor linkers are governed by the backward stepping rate $2\beta(F\{\sigma_2\})$, where the prefactor 2 arises because a change in the step number $\sigma_2 \to \sigma_2 \pm \frac{1}{2}$ can be a result of two independent events in the fine-grained descripition: $s_1 \to s_1 \pm 1$ or $s_2 \to s_2 \pm 1$. Similarly, the transition from the activity state $(n = 2)$ to $(n = 1)$ is governed by the effective unbinding rate $2\epsilon(\langle \mathcal{F}_2 \rangle/2)$ due to the two independent events of motor unbinding. Fig. S2(c) represents the coarse-grained state space with the corresponding transition rates between activity states as well as their elastic substates. The coarse-graining algorithm is based on calculating the steady state probabilities for the activity states and their elastic substates separately, and subsequently reweighting the probabilities of all substates by the probabilities of the activity states to obtain the average forces $\langle \mathcal{F}_N^* \rangle$.

S3 Details for kinesin-1 data compared with experiments

Here we provide details for the simulation data from Fig. 4 of the main text, which we used to compare with experiments on kinesin-1 from Ref. (27). Fig. S3 displays the relative frequencies (a) of the number of active motors, and (b) of the maximum separation between the leading and the trailing motor in each activity state (n) measured in units of the step size ℓ. We observe that the probability to find a large number of active motors decreases strongly with n, see Fig. S3(a). For $N = 4$ available motors, the force generation is mainly performed *via* the action of one or two active kinesin motors. Furthermore, the distributions in (b) indicate that active motors are typically separated by at most 2 steps.

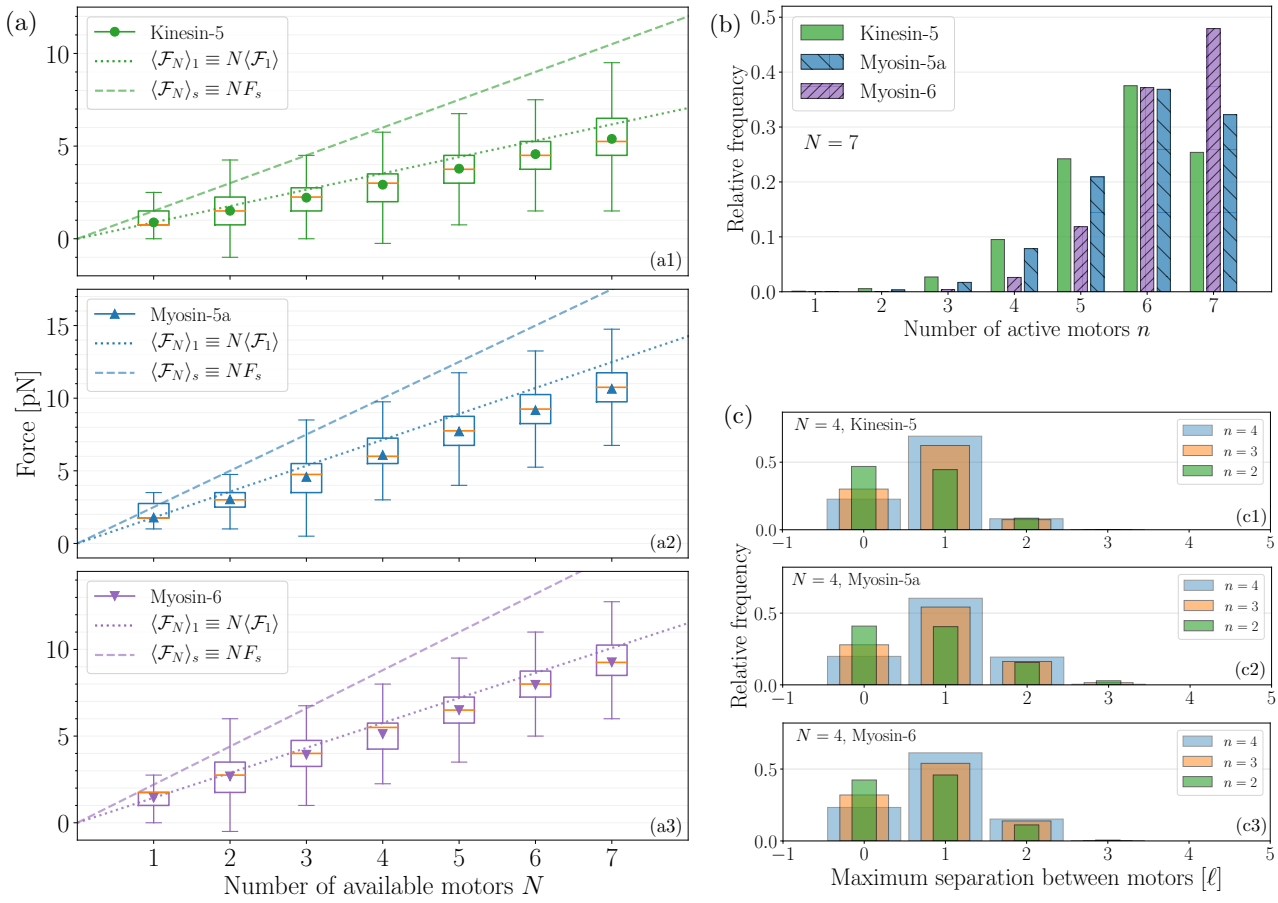

Figure S4: Collective force generation by teams of (a1) kinesin-5, (a2) myosin-5a and (a3) myosin-6 motors consisting of up to $N = 7$ motors. Force distributions are represented as box plots with mean values given by triangular and circular markers, and medians by horizontal lines (orange); whiskers indicate 1.5 interquartile range. The force scale $\langle \mathcal{F}_N \rangle_1$ and the collective stall force $\langle \mathcal{F}_N \rangle_s$ are delineated by dotted and dashed lines in each plot, respectively. The three types of motors have stall forces of $F_s \leq 2.5\,\mathrm{pN}$, see Table S1, and their average forces are close to the force scale $\langle \mathcal{F}_1 \rangle_1$. Average forces of kinesin-5 (a1) are somewhat closer to its collective stall force $\langle \mathcal{F}_N \rangle_s$ compared with the average forces of myosin-5a (a2) and myosin-6 (a3). (b) Relative frequencies of different activity states with n active motors for a total number of $N = 7$ available motors reveal that all three types of motors have high probabilities for having a large number of active motors. (c1-c3) Relative frequencies of the maximum separation between the leading and the trailing motor measured in units of the step size ℓ for a total number of $N = 4$ available motors. The distributions indicate that active motors are typically separated by at most a single step.

S4 Force distributions of kinesin-5, myosin-V and myosin-VI

In Fig. 5 of the main text we show the rescaled average forces $\langle \mathcal{F}_N \rangle / F_s$ for different teams consisting of up to $N = 7$ motors. The distributions from which these average forces are calculated are shown in Fig. 3 of the main text for kinesin-1, strong dynein and weak dynein. In Fig. S4 we present the corresponding distributions for the three remaining motor types analyzed in the main text: kinesin-5, myosin-5a and myosin-6. In all three cases, the average collective forces $\langle \mathcal{F}_N \rangle$ are very close to the force scale $\langle \mathcal{F}_N \rangle_1 \equiv N\langle \mathcal{F}_1 \rangle$, see Fig. S4(a1-a3). For $N = 7$ available motors, the three types of motors have high probabilities to find a large number n of active motors, as determined by the relative frequencies displayed in Fig. S4(b). In fact, the most likely activity state for myosin-6 is one where all available motors are bound to the track. Figs. S4(c1-c3) display the relative frequencies for the maximum separation between the leading and the trailing motor for different numbers $n = 2, 3, 4$ of active motors in a team with $N = 4$ motors. The distances is measured in units of the step size ℓ. Note

that for kinesin-5 the step size is $\ell = 8\,\mathrm{nm}$, whereas the myosin motors have $\ell = 36\,\mathrm{nm}$, see Table S1. These distributions show that active motors are typically separated by at most a single step.

S5 Parameter dependence for a test motor

To understand how the collective forces depend on the single motor parameters, we performed simulations for a test motor by changing one parameter value at a time. The reference parameter set for the test motor is identical with the parameter set of kinesin-1, see Table S1. The changed parameter values are specified in the inset of Fig. S5.

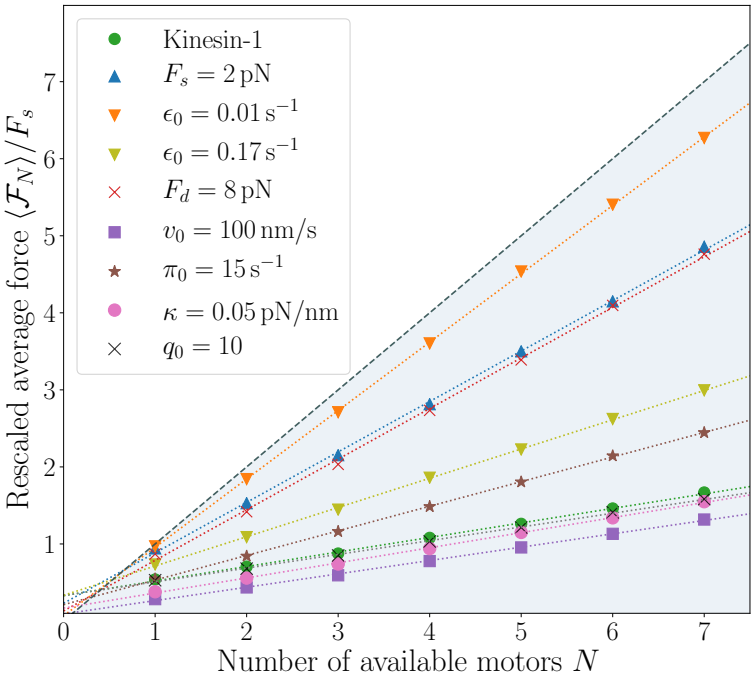

Figure S5: Dependence of the collective forces on the single motor parameters for teams consisting of different numbers N of available motors. The reference parameter set corresponds to that of kinesin-1 (green circles), see Table S1, and the values for the changed parameters are specified in the inset. The average collective forces $\langle \mathcal{F}_N \rangle$ for different N are rescaled by the single motor stall force F_s. A low zero-force unbinding rate of $\epsilon_0 \simeq 0.01\,\mathrm{s}^{-1}$ (downward-pointing triangles) is sufficient to convert kinesin-1's sub-additive collective force generation into additive force generation with $\langle \mathcal{F}_N \rangle \simeq \langle \mathcal{F}_N \rangle_s \equiv N F_s$. Likewise, reducing the stall force (upward-pointing triangles), increasing the detachment force F_d (red crosses) or the rebinding rate π_0 (stars) leads to better cooperativity in force generation. The four parameters F_s, F_d, ϵ_0 and π_0 have the strongest impact on the collective force, while this force depends most strongly on the stall force F_s and the detachment force F_d when these parameters are changed by a similar factor. Reducing the zero-force velocity v_0 (squares) leads to a moderate decrease in the collective average forces, which depend even more weakly on changes in the stiffness κ and the zero-force stepping ratio q_0.

Fig. S5 displays the parameter dependence of the collective force values for motor teams consisting of N available motors. We observe that the average forces of kinesin-1 can approach its collective stall force NF_s by reducing the zero-force unbinding rate ϵ_0 from $0.66\,\mathrm{s}^{-1}$ to $0.01\,\mathrm{s}^{-1}$. A high detachment force F_d has a similar effect, however, the zero-force unbinding rate ϵ_0 can be directly modified in experiments by changing the buffer conditions. We note that a reduction of ϵ_0 by the same factor as that of the detachment force leads to a more moderate change in the collective forces, see the data points for $\epsilon_0 = 0.17\,\mathrm{s}^{-1}$.We furthermore observe that collective force generation of kinesin-1 also becomes more additive when its stall force F_s is reduced from 7 pN to 2 pN, and when the rebinding rate π_0 of a single motor is increased. The absolute values of the collective average forces $\langle \mathcal{F}_N \rangle$ for

variations in ϵ_0- and F_d-values are approximately 44 pN and 33 pN for $N = 7$, respectively. The former value is quite close to the collective stall force $NF_s = 49$ pN of a team of $N = 7$ kinesin-1 motors, which indicates that such high force values could be in principle observed *in vitro* by changing the ion concentrations.

Reducing the zero-force velocity v_0 of kinesin-1 leads to a small overall decrease in the collective average forces. The average single motor force for this case is around $\langle \mathcal{F}_1 \rangle \simeq 2$ pN, whereas the reference average single motor force is about 3.8 pN; the average forces for $N = 7$ are 9.2 pN and 11.7 pN for the reduced velocity and for the reference motor, respectively. Therefore, low v_0-values in general lead to lower average forces, but the collective average forces become closer to the force scale $N\langle \mathcal{F}_1 \rangle$ because of the low single motor average force. We observe that changing the stiffness κ or the stepping ratio q_0 has a weak effect on the collective average forces.

We next study the dependence of the collective average force $\langle \mathcal{F}_N \rangle$ to changes in the force parameters F_s and F_d more closely to see whether the force ratio $f \equiv F_s/F_d$ can be systematically used to distinguish between strong and weak motors. We use the coarse-grained model to obtain the average collective forces $\langle \mathcal{F}_N^* \rangle$ for $N = 3$ and rescale these by NF_s such that $\langle \mathcal{F}_N^* \rangle / NF_s$ varies between 0 and 1. All parameters apart from F_s and F_d take the values corresponding to kinesin-1, see Table S1. In Fig. S6, we observe that the rescaled force $\langle \mathcal{F}_N^* \rangle / NF_s$ depends inversely on the force ratio f: Large and small values of f in general correspond to small and large values of the rescaled average force, respectively. Furthermore, for fixed values of the force ratio f and for small F_s, the rescaled forces $\langle \mathcal{F}_N^* \rangle / NF_s$ remain approximately constant and slightly increase for large F_s.

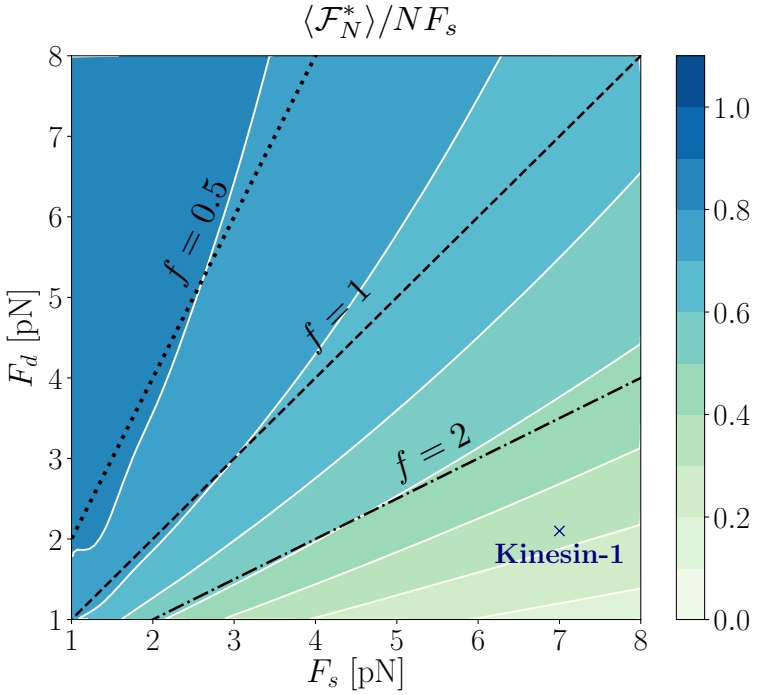

Figure S6: Dependence of collective average forces $\langle \mathcal{F}_N^* \rangle$ rescaled by NF_s for $N = 3$ on the parameters F_s and F_d, obtained from the coarse-grained model. The remaining parameters take the values corresponding to kinesin-1, see Table S1. The data point (cross) denotes the F_s- and F_d-values of kinesin-1. The straight lines indicate different values of the force ratio $f \equiv F_s/F_d$. Moving along fixed f-values, one can approximately maintain a constant value for the rescaled force $\langle \mathcal{F}_N^* \rangle / NF_s$ for small F_s.

S6 Different forms of the force-velocity relation

To clarify the question whether the specific form of the force-velocity relation $v(F)$ of a single motor predominantly determines the collective force generation mechanism, we investigate collective forces of motors with a convex (or concave-upward) and concave (or convex-downward) force-velocity curve and compare the collective forces with those of kinesin-1 teams. We obtain the convex and concave force-velocity curves by changing the values of the maximum and minimum velocity paramaters $v_{\max}$ and $v_{\min}$. The convex and concave force-velocity relations, as well as that of kinesin-1 are plotted in Fig. S7.

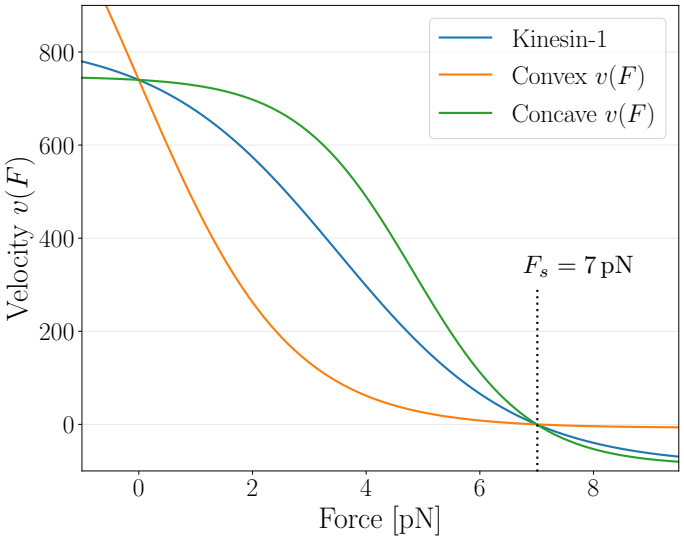

Figure S7: Force-velocity relation of kinesin-1, and modified force-velocity relations of kinesin-1 with a convex and concave form. For the convex case, we used the parameter values $v_{\max} = 2v_0 = 1480\,\mathrm{nm/s}$ and $v_{\min} = -0.01v_0 = -7.4\,\mathrm{nm/s}$, whereas for the concave case we used $v_{\max} = 1.01v_0 = 747.4\,\mathrm{nm/s}$ and $v_{\min} = -0.12v_0 = -88.8\,\mathrm{nm/s}$. The remaining parameters take those of kinesin-1, see Table S1, with the stall force given by $F_s = 7\,\mathrm{pN}$, (dotted line).

In Fig. S8 we display collective forces generated by the two types of motors with a modified force-velocity relation compared with the forces of kinesin-1. Figs. S8(a2-a3) indicate that the sub-additive force generation mechanism of kinesin-1, see Fig. S8(a1), does not change markedly with modifications in the specific form of the force-velocity relation $v(F)$. In all three cases, average forces generated for a team of $N = 7$ motors are around $\langle \mathcal{F}_N \rangle \simeq 12\,\mathrm{pN}$. Nevertheless, we observe that the force distributions are somewhat narrower for motors with a convex force-velocity curve, compared with those of kinesin-1 and with the concave case. Additionally, relative frequencies of activity states (n), see Fig. S8(b), show that for motors with a convex $v(F)$ the average number of active motors are slightly higher than for kinesin-1 and for the concave case. Finally, for kinesin-1 (c1) and for the concave case (c2), the maximum separation between the leading and the trailing motor is typically given by at most 2 steps. Motors with a convex $v(F)$ (c3), on the other hand, are typically separated by at most a single step, which indicates that these motors share their overall load slightly more equally as compared with kinesin-1 and with the concave-up case. However, this improvement in the force sharing configurations does not significantly modify the collective force generation mechanism, as shown in Figs. S8(a1-a3).

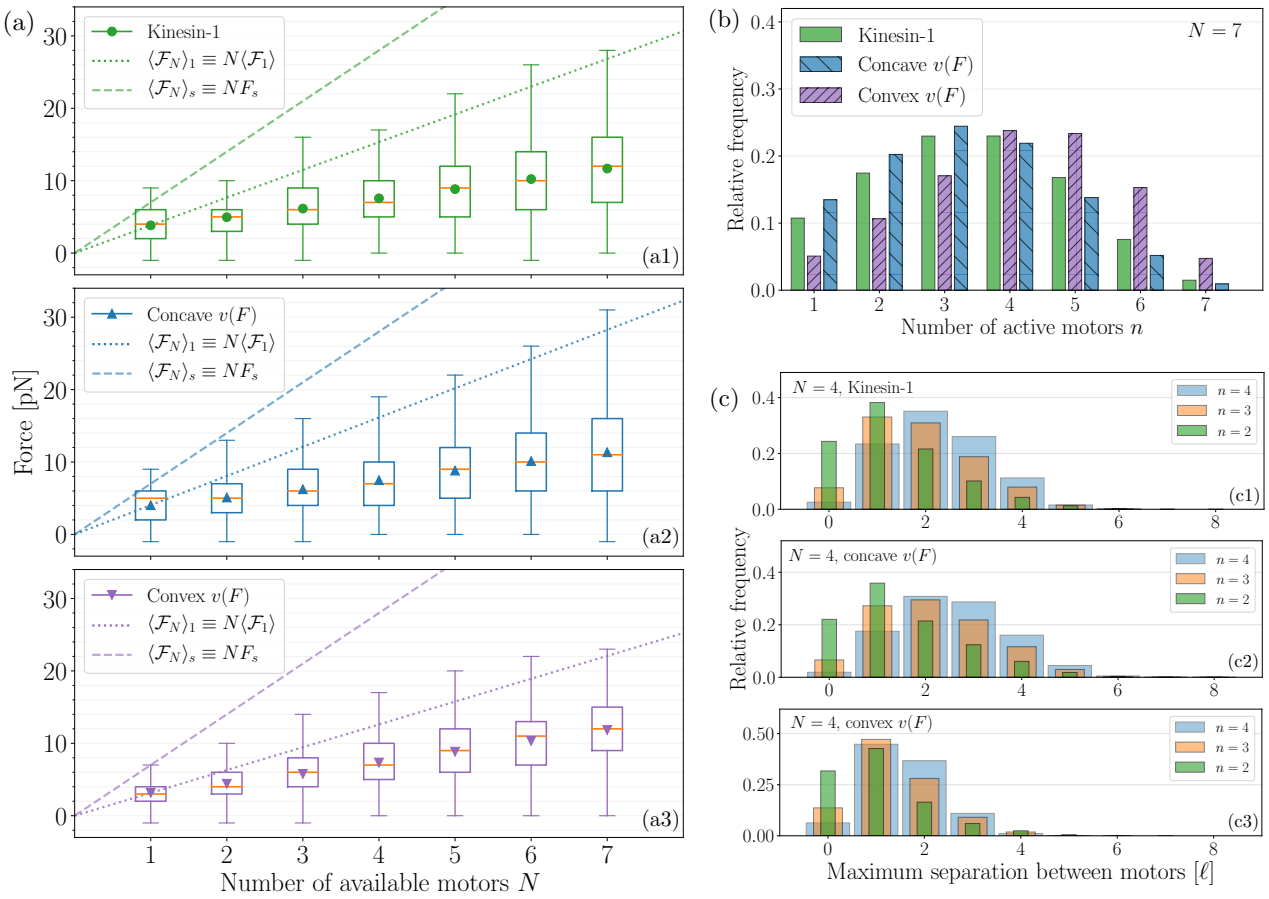

Figure S8: Collective force generation by teams of (a1) kinesin-1 motors, compared with motors with (a2) convex and (a3) concave force-velocity relations $v(F)$, see Fig. S7 for the corresponding $v(F)$-relations. Force distributions are represented as box plots with mean values given by triangular and circular markers, and medians by horizontal lines (orange); whiskers indicate 1.5 interquartile range. Collective average forces $\langle \mathcal{F}_N \rangle$ for all three cases take similar values, whereas the distributions for the convex case are narrower compared with kinesin-1 and with the concave case. (b) Relative frequencies of the different activity states (n) for $N = 7$ available motors indicate that the average number of active motors slightly increases for the convex-up case compared with kinesin-1 and with the concave case. (c1-c3) Distributions for the maximum separation between the leading and the trailing motor given in units of the step size ℓ. Motors with a convex force-velocity relation $v(F)$ share the overall load slightly more equally than teams of kinesin-1 and motors with a concave $v(F)$, because the latter have broader distributions for the maximum separation.

References

(1) Uçar MC, Lipowsky R. Force sharing and force generation by two teams of elastically coupled molecular motors. Sci Rep. 2019;9(1):454.

(2) Berger F, Keller C, Klumpp S, Lipowsky R. Distinct transport regimes for two elastically coupled molecular motors. Phys Rev Lett. 2012;108(20):208101.

(3) Uçar MC, Lipowsky R. Tug-of-war between two elastically coupled molecular motors: a case study on force generation and force balance. Soft Matter. 2017;13:328–344.

(4) Carter NJ, Cross R. Mechanics of the kinesin step. Nature. 2005;435(7040):308–312.

(5) Kramers H. Brownian motion in a field of force and the diffusion model of chemical reactions. Physica. 1940;7:284.

(6) Klumpp S, Keller C, Berger F, Lipowsky R. Molecular motors: Cooperative phenomena of mul-

tiple molecular motors. In: Multiscale Modeling in Biomechanics and Mechanobiology. Springer; 2015. p. 27–61.

(7) Andreasson JO, Milic B, Chen GY, Guydosh NR, Hancock WO, Block SM. Examining kinesin processivity within a general gating framework. eLife. 2015;4.

(8) Berger F, Klumpp S, Lipowsky R. Force-dependent unbinding rate of molecular motors from stationary optical trap data. Nano Lett. 2019;.

(9) King SJ, Schroer TA. Dynactin increases the processivity of the cytoplasmic dynein motor. Nat Cell Biol. 2000;2(1):20–24.

(10) Ali MY, Kennedy GG, Safer D, Trybus KM, Sweeney HL, Warshaw DM. Myosin Va and myosin VI coordinate their steps while engaged in an in vitro tug of war during cargo transport. Proc Natl Acad Sci U S A. 2011;108(34):E535–E541.

(11) Leduc C, Campas O, Zeldovich KB, Roux A, Jolimaitre P, Bourel-Bonnet L, et al. Cooperative extraction of membrane nanotubes by molecular motors. Proc Natl Acad Sci U S A. 2004;101(49):17096–17101.

(12) Toba S, Watanabe TM, Yamaguchi-Okimoto L, Toyoshima YY, Higuchi H. Overlapping hand-over-hand mechanism of single molecular motility of cytoplasmic dynein. Proc Natl Acad Sci U S A. 2006;103(15):5741–5745.

(13) Gennerich A, Carter AP, Reck-Peterson SL, Vale RD. Force-induced bidirectional stepping of cytoplasmic dynein. Cell. 2007;131(5):952–965.

(14) Rai AK, Rai A, Ramaiya AJ, Jha R, Mallik R. Molecular adaptations allow dynein to generate large collective forces inside cells. Cell. 2013;152(1):172–182.

(15) Blehm BH, Schroer TA, Trybus KM, Chemla YR, Selvin PR. In vivo optical trapping indicates kinesin's stall force is reduced by dynein during intracellular transport. Proc Natl Acad Sci U S A. 2013;110(9):3381–3386.

(16) Shimamoto Y, Forth S, Kapoor TM. Measuring pushing and braking forces generated by ensembles of kinesin-5 crosslinking two microtubules. Dev Cell. 2015;34(6):669–681.

(17) Fallesen T, Roostalu J, Duellberg C, Pruessner G, Surrey T. Ensembles of Bidirectional Kinesin Cin8 Produce Additive Forces in Both Directions of Movement. Biophys J. 2017;113(9):2055–2067.

(18) Uemura S, Higuchi H, Olivares AO, De La Cruz EM, Ishiwata S. Mechanochemical coupling of two substeps in a single myosin V motor. Nat Struct Mol Biol. 2004;11(9):877.

(19) Gebhardt JCM, Clemen AEM, Jaud J, Rief M. Myosin-V is a mechanical ratchet. Proc Natl Acad Sci U S A. 2006;103(23):8680–8685.

(20) Watanabe TM, Iwane AH, Tanaka H, Ikebe M, Yanagida T. Mechanical characterization of one-headed myosin-V using optical tweezers. PLoS One. 2010;5(8):e12224.

(21) Altman D, Sweeney HL, Spudich JA. The mechanism of myosin VI translocation and its load-induced anchoring. Cell. 2004;116(5):737–749.

(22) McKenney RJ, Vershinin M, Kunwar A, Vallee RB, Gross SP. LIS1 and NudE induce a persistent dynein force-producing state. Cell. 2010;141(2):304–314.

(23) Rogers AR, Driver JW, Constantinou PE, Jamison DK, Diehl MR. Negative interference dominates collective transport of kinesin motors in the absence of load. Phys Chem Chem Phys. 2009;11(24):4882–4889.

(24) Oiwa K, Sakakibara H. Recent progress in dynein structure and mechanism. Curr Opin Cell Biol. 2005;17(1):98–103.

(25) Reck-Peterson SL, Yildiz A, Carter AP, Gennerich A, Zhang N, Vale RD. Single-molecule analysis of dynein processivity and stepping behavior. Cell. 2006;126(2):335–348.

(26) Valentine MT, Fordyce PM, Krzysiak TC, Gilbert SP, Block SM. Individual dimers of the mitotic kinesin motor Eg5 step processively and support substantial loads in vitro. Nat Cell Biol. 2006;8(5):470.

(27) Furuta K, Furuta A, Toyoshima YY, Amino M, Oiwa K, Kojima H. Measuring collective transport by defined numbers of processive and nonprocessive kinesin motors. Proc Natl Acad Sci U S A. 2013;110(2):501–506.

(28) Gillespie DT. Markov processes: An introduction for physical scientists. Elsevier; 1991.